Environmental Science & Technology

Article

pubs.acs.org/est

Mercury Emission Ratios from Coal-Fired Power Plants in the Southeastern United States during NOMADSS

Jesse L. Ambrose,[*,†] Lynne E. Gratz,[†] Daniel A. Jaffe,[†,‡] Teresa Campos,[§] Frank M. Flocke,[§] David J. Knapp,[§] Daniel M. Stechman,[§] Meghan Stell,[§] Andrew J. Weinheimer,[§] Christopher A. Cantrell,[∥] and Roy L. Mauldin III[∥,⊥]

[†]School of Science, Technology, Engineering, and Mathematics, Physical Sciences Division, University of Washington, Bothell, Washington 98011, United States

[‡]Department of Atmospheric Sciences, University of Washington, Seattle, Washington 98195, United States

[§]Atmospheric Chemistry Observations & Modeling Laboratory, National Center for Atmospheric Research, Boulder, Colorado 80307, United States

[∥]Department of Atmospheric and Oceanic Sciences, University of Colorado, Boulder, Colorado 80309, United States

[⊥]Department of Physics, University of Helsinki, Helsinki FI-00014, Finland

Supporting Information

ABSTRACT: We use measurements made onboard the National Science Foundation's C-130 research aircraft during the 2013 Nitrogen, Oxidants, Mercury, and Aerosol Distributions, Sources, and Sinks (NOMADSS) experiment to examine total Hg (THg) emission ratios (EmRs) for six coal-fired power plants (CFPPs) in the southeastern U.S. We compare observed enhancement ratios (ERs) with EmRs calculated using Hg emissions data from two inventories: the National Emissions Inventory (NEI) and the Toxics Release Inventory (TRI). For four CFPPs, our measured ERs are strongly correlated with EmRs based on the 2011 NEI (r^2 = 0.97), although the inventory data exhibit a −39% low bias. Our measurements agree best (to within ±32%) with the NEI Hg data when the latter were derived from on-site emissions measurements. Conversely, the NEI underestimates by approximately 1 order of magnitude the ERs we measured for one previously untested CFPP. Measured ERs are uncorrelated with values based on the 2013 TRI, which also tends to be biased low. Our results suggest that the Hg inventories can be improved by targeting CFPPs for which the NEI- and TRI-based EmRs have significant disagreements. We recommend that future versions of the Hg inventories should provide greater traceability and uncertainty estimates.

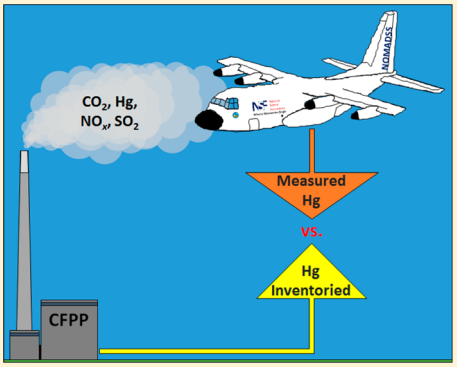

INTRODUCTION

According to contemporary inventories, exhaust from the combustion of fossil fuel (mainly coal), biofuel, and waste in stationary combustion sources (e.g., utility and industrial boilers) comprises 35−77% of anthropogenic Hg emissions to the atmosphere worldwide.[1−5] On a global basis, coal-fired power plants (CFPPs) in particular are estimated to account for most (≥56%) of the Hg emitted by stationary combustion sources.[5,6] In the U.S., recent estimates attribute 56% of all anthropogenic Hg emissions to stationary combustion sources and 87% of all Hg emissions from stationary combustion sources to CFPPs.[7] (See the Supporting Information for further details.)

For 1990 and subsequent years, the total magnitudes of worldwide atmospheric Hg emissions from stationary combustion sources are considered to be relatively well-constrained, with uncertainties usually quoted at ±25%.[1−3,5,8−12] The associated Hg emissions speciation (i.e., the distribution of elemental and oxidized Hg) and in-plume atmospheric chemical processing are less well-characterized.[13−20] In general, emissions estimates are assumed to be most accurate for Europe, Canada, and the U.S. because of long-standing inventory development for those regions.[2,3,21] However, emissions estimates for individual facilities are more uncertain when they are not based on on-site emissions testing.[22]

Mercury emissions data for stationary combustion sources and other point sources in the U.S. are quantified in two inventories by the U.S. Environmental Protection Agency (EPA): the National Emissions Inventory (NEI)[23] and the Toxics Release Inventory (TRI).[24] The NEI, which includes more detailed emissions data than the TRI, is regarded as more accurate[25] and is often the primary source of U.S. Hg emissions data used in global emissions inventories[2,3,5] and in chemical transport models[15,17,26−30] (CTMs). In both inventories, emissions estimates for individual point sources are provided

Received: April 7, 2015
Revised: June 30, 2015
Accepted: July 10, 2015

DOI: 10.1021/acs.est.5b01755
Environ. Sci. Technol. XXXX, XXX, XXX−XXX

without uncertainty parameters. (Further details on the NEI and TRI are provided below and in the Supporting Information.)

Few studies have compared bottom-up Hg emissions estimates for individual CFPPs with top-down estimates based on in-plume atmospheric measurements.[13,14,19,20] All of these studies focused on emissions speciation rather than absolute emission magnitudes, and none considered emissions data reported in the NEI and TRI. Similarly, most efforts to reconcile discrepancies between atmospheric observations and predictions from atmospheric CTMs focus on adjusting the speciation and/or atmospheric chemical processing of Hg emissions, while treating total emissions as fixed parameters.[17,18,26,30,31] Independent evaluations of the Hg inventories are needed, including quantification of total emissions from stationary combustion sources on the basis of in-plume atmospheric measurements.

In this study, we quantify total Hg (THg) enhancement ratios (ERs) for six CFPPs in the southeastern United States using atmospheric measurements made from onboard the National Science Foundation's (NSF's) C-130 research aircraft. The measured ERs are then compared with emission ratios (EmRs) from the NEI and TRI. Though based on a limited data set, the results are relevant to many applications of the Hg inventories, including their use in atmospheric CTMs.

EXPERIMENTAL SECTION

NOMADSS Experiment. Measurements reported here were made over the southeastern U.S. during June and July 2013 from onboard the NSF's C-130 aircraft as part of the Nitrogen, Oxidants, Mercury, and Aerosol Distributions, Sources, and Sinks (NOMADSS) field campaign. The NOMADSS experiment was one component of the Southeast Atmosphere Study (SAS), which was a regional atmospheric chemistry and climate study that employed several aircraft-based observing platforms, a network of ground-based observing stations, and extensive CTM efforts.[32]

The main NOMADSS science goals related to Hg were to quantify emissions from several large U.S. Hg point sources, and to characterize the distribution and chemistry of atmospheric Hg over the southeastern United States. The first goal is addressed here. The second goal is addressed in Gratz et al.[33] and Shah et al.,[34] which use the GEOS-Chem[31] global CTM to diagnose the sources of large oxidized Hg enhancements that we observed in the free troposphere. Additionally, Song et al.[35] use the NOMADSS observations and GEOS-Chem to constrain terrestrial and marine atmospheric Hg fluxes.

Instrumentation, Hg: Overview. Measurements of THg, gaseous elemental mercury (GEM), and oxidized mercury (Hg^{II}) were made using the University of Washington's Detector for Oxidized Hg Species (DOHGS). The design and operating principles of the DOHGS are described in detail in Ambrose et al.[36] and in the Supporting Information. Therefore, we provide only a brief instrument review here, focusing on the latest modifications.

During NOMADSS, the DOHGS was configured as described in Lyman and Jaffe,[37] with modifications to the cold-vapor atomic fluorescence spectrophotometers (CVAFSs) and the GEM analytical channel as described in Ambrose et al.[36] Soda-lime traps[36] were installed upstream of the CVAFSs to guard the Hg preconcentration traps from acid gases.[38] Modifications carried out in preparation for NOMADSS are discussed in the Supporting Information.

Instrumentation, Hg: Calibration and Uncertainties. The DOHGS was calibrated, concentrations of THg, GEM, and Hg^{II} were quantified, and measurement uncertainties were estimated as described in Ambrose et al.,[36] with minor procedural and computational differences as described below and in the Supporting Information. Concentrations of Hg^{II} observed in the plumes presented here were very near to or below the 3σ limit of detection (LOD; 0.06–0.12 ng/m^3 for the flights discussed here). We therefore present only our measurements of THg, which are directly comparable to the Hg emissions data reported in the NEI and TRI. (The GEM and Hg^{II} measurements are described in the Supporting Information.)

Total Hg was sampled continuously (as GEM) using two alternating Au preconcentration traps; the sample integration time and the measurement time resolution were 150 s. Calibration and zeroing were carried out separately for each flight using measurements made in-flight and on the ground pre- and postflight. The mean 1σ precision and calibration uncertainty for THg were ±3.6 and ±6.8%, respectively, for concentrations well above the LOD (0.067 ng/m^3, 3σ). Overall uncertainty was conservatively estimated as the sum of 1σ precision and calibration uncertainty.

Instrumentation, Additional Measurements. An extensive suite of atmospheric parameters was measured from onboard the C-130 during NOMADSS.[32] Here, we describe only the key supporting measurements used in this study. Measurements of carbon dioxide (CO_2) were made at 5 Hz (recorded as 1 s averages) with a PICARRO Model G1301-f infrared cavity ring-down spectrometer; 1σ precision (at 5 Hz) and calibration uncertainty were both ±0.25 ppmv. Measurements of SO_2 were made at 1 Hz (recorded as 10 s averages) using a Thermo Scientific Model 43*i*-TLE pulsed-fluorescence gas analyzer; 1σ precision (at 0.1 Hz) and calibration uncertainty were ±22.5% and the larger of 15% of the observed value and the LOD (150 pptv, 2σ), respectively. Measurements of nitric oxide (NO) and nitrogen dioxide (NO_2) were made at 10 Hz (recorded as 1 s averages) using a two-channel NO + ozone (O_3) chemiluminescence instrument,[39] where NO_2 was photolytically converted to NO prior to detection;[40] overall uncertainties (at 1 Hz) were taken to be the larger of 10% for NO (15% for NO_2) and the LOD (10 pptv for NO; 20 pptv for NO_2), respectively. Measurements of hydroxyl radical (HO·) were made at 5 Hz for 8 s out of every 15 s (values reported as 30 s averages) by chemical ionization mass spectrometry (CIMS) using $NO_3^-{\cdot}HNO_3$ cluster ions as the ionizing reagent;[41] overall uncertainty (at 0.03 Hz) was ±22.5%. State parameters, including ambient temperature, pressure, aircraft location (latitude, longitude, and altitude), and horizontal wind vectors, were measured at 5 Hz (recorded as 1 s averages) by the aircraft's instrumentation.[42] Overall uncertainties in these measurements are estimated to be ±0.2 °C, ± 0.2 mbar, ± 100 m, ± 100 m, ± 10 m above mean sea level (AMSL), and ±0.5 m/s, respectively.[43]

When averaging high time resolution (i.e., 1 and 0.1 Hz) measured values to longer time intervals, precisions quoted above were scaled by $n^{-0.5}$, where n represents the number of measurements averaged, in order to approximate the precision in the lower time resolution means.

Emissions Inventories. To identify the sources of pollution plumes we sampled and to draw comparisons against

DOI: 10.1021/acs.est.5b01755
Environ. Sci. Technol. XXXX, XXX, XXX–XXX

our top-down Hg emissions estimates, we used four emissions inventories prepared by the EPA: the Air Markets Program Data (AMPD) database,[44] the National Emissions Inventory,[23] the Toxics Release Inventory,[24] and the Greenhouse Gas Reporting Program (GHGRP) database.[45] The AMPD database reports hourly CO_2, SO_2, and NO_x emissions data for large (>25 MW) fossil-fuel-fired power plants. The data are retrievable at hourly, monthly, and annual frequencies. The NEI reports annual criteria air pollutant (CAP) and hazardous air pollutant (HAP) emissions data for all air emissions sources, with triennial reporting frequency. For this study, the latest NEI reporting year was 2011. The TRI reports annual HAP emissions data for industrial point sources in specific sectors that exceed thresholds for size and material throughput; the data are reported with annual frequency.[46] The GHGRP database reports annual greenhouse gas (e.g., CO_2) emissions data for large industrial point sources, with annual reporting frequency. (Further details on the inventories are provided in the Supporting Information.)

From the AMPD database, we used hourly CO_2, NO_x, and SO_2 emissions data for the NOMADSS campaign period and annual data for the years 2011 and 2013. From the GHGRP database, we used annual CO_2 emissions data for 2013. From the NEI, we used annual Hg emissions data for 2011. From the TRI, we used annual Hg emissions data for 2011 and 2013. We also used Hg emissions data compiled by the EPA for CFPPs during development of the Mercury and Air Toxics Standards (MATS) rule;[47] the MATS data underlie many of the Hg emissions estimates for CFPPs reported in the 2011 NEI, including those for the CFPPs we sampled during NOMADSS (discussed below).

Discrepancies between the NEI and TRI data partly reflect differences in the emissions estimation methods underlying each inventory.[23,48] The TRI includes emissions estimates reported to the EPA by the emitting facilities, whereas the NEI mostly includes emissions estimates made by the EPA. Because the EPA plays a much more active role in developing the emissions estimates reported in the NEI, the NEI data are expected to be more accurate when both inventories report emissions estimates for the same source.[49] However, emissions estimates for individual facilities are particularly uncertain in the absence of direct emissions testing,[22] and neither inventory provides quantitative uncertainty bounds with the emissions data reported.

The level of consistency between the NEI and TRI Hg data is illustrated in Figure 1, which compares the 2011 Hg emissions reported for CFPPs by both inventories. (See Supporting Information for further details.) The TRI exhibits a statistically significant 20% positive bias with respect to the NEI. (The bias appears to be influenced disproportionately by a small number of high Hg-emitting facilities.) The correlation between the two inventories is fair, with 37% of the variability unexplained. Of the CFPPs we sampled during NOMADSS (discussed below; labeled values in Figure 1), Big Brown Station and Dolet Hills Station showed the poorest agreement; the corresponding relative differences (≡ 100 × difference ÷ mean) between the NEI- and TRI-based Hg emission estimates were −177 and 80%, respectively. For the remaining sampled CFPPs, the relative differences fell within ±25%. Welsh Power Plant showed the best agreement (relative difference = 17%) between the two inventories. The reliability of each inventory for predicting emissions in real time, however, cannot be assessed without independent, top-down evaluation.

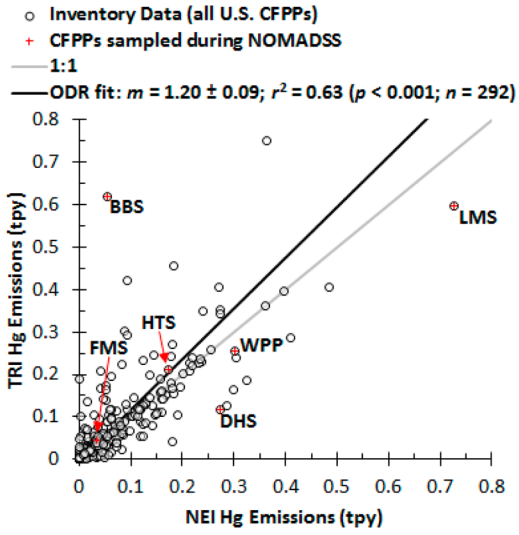

Figure 1. Comparison of annual (2011) atmospheric Hg emissions (tons per year, tpy) reported for CFPPs in both the NEI and TRI; CFPPs sampled during NOMADSS are labeled. The fit includes all CFPPs and was calculated by unweighted linear orthogonal distance regression (ODR). Uncertainty in the slope is 95% confidence interval (CI). The intercept (−0.00 ± 0.01 tpy) is not significantly different from zero at 95% CI. Facility abbreviations: BBS, Big Brown Station; DHS, Dolet Hills Station; FMS, Fort Martin Station; HTS, Hatfield Station; LMS, Limestone Station; WPP, Welsh Power Plant.

Source Identification for Pollution Plumes Sampled by the C-130. Figure 2 shows the procedures used to compare

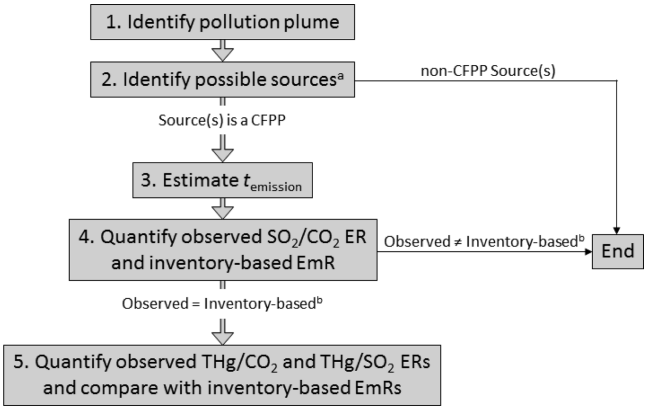

Figure 2. Procedures we used to identify the sources of Hg-rich pollution plumes sampled during NOMADSS. In this study, we quantify Hg enhancement ratios (ERs) and emission ratios (EmRs) only for CFPPs (step 5). (a) Using measured winds and HYSPLIT. (b) To within calculated uncertainties.

the observed ERs with the inventory-based EmRs. Pollution plume encounters were identified in the C-130 time series as concurrent enhancements in THg and copollutants, including SO_2, which we used as a tracer of high Hg-emitting sources (e.g., CFPPs), and the more general combustion tracers CO, CO_2, and NO_x (step 1; example data, Figure S2). All plumes presented here were sampled in the boundary layer at altitudes between 0.4 and 1.4 km AMSL.

When identifying possible upwind sources, we conducted plume dispersion modeling using the National Oceanic and Atmospheric Administration's (NOAA's) HYbrid Single-Particle Lagrangian Integrated Trajectory (HYSPLIT) model

DOI: 10.1021/acs.est.5b01755
Environ. Sci. Technol. XXXX, XXX, XXX−XXX

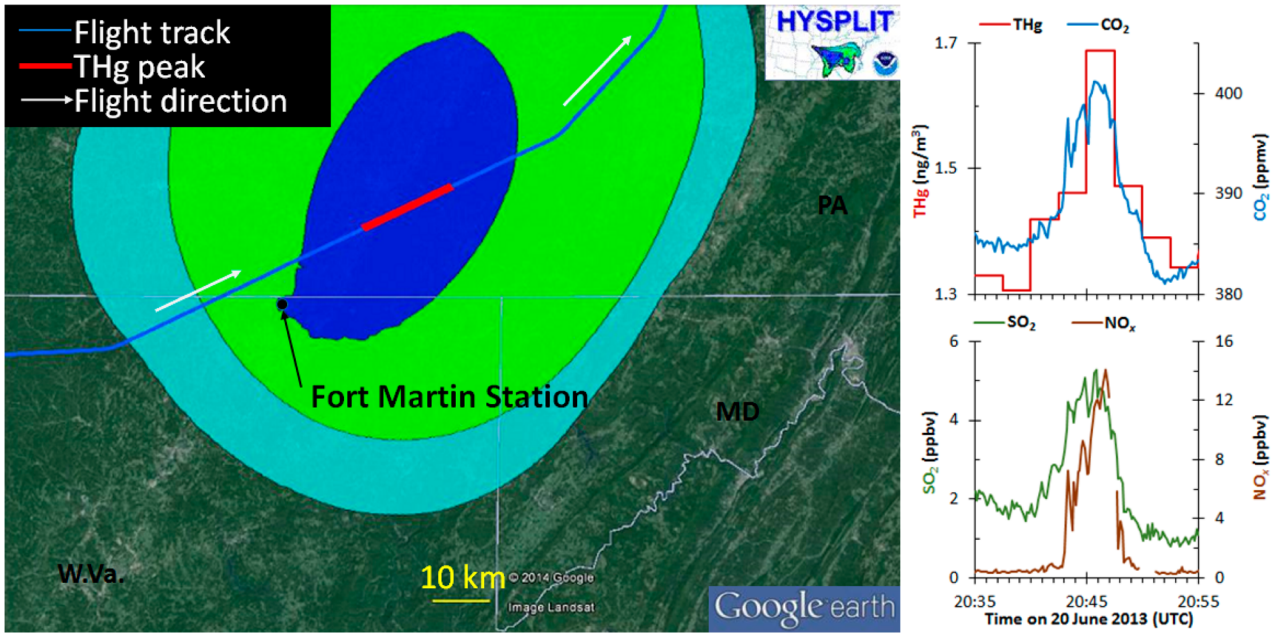

Figure 3. (left) The C-130 flight track from RF-07 is shown, overlaid on HYSPLIT-modeled plume dispersion from the upwind Fort Martin CFPP. The plot boundaries intersect the flight track at 20:35 and 20:55 UTC. At right, selected measurements made along the flight track are shown. The modeled and observed plume centers (at 2.5 min resolution) were encountered between 20:45 and 20:47:30 UTC (red bar in the left panel).

(step 2, Figure 2).[50] (See the Supporting Information for further details.) Figure 3 shows an example of modeled plume dispersion from the Fort Martin CFPP for research flight seven (RF-07), along with measured tracer species from the C-130.

When the procedures above identified a CFPP as the possible source of an observed plume, the measured horizontal wind velocities, v_{wind}, and the horizontal distances, d_{source}, between the points of sampling along the flight track and the source coordinates were used to estimate the corresponding mean plume transport time since emission, Δt_{plume}, and the emission time, $t_{emission}$ (step 3, Figure 2). Overall uncertainty in $t_{emission}$, $\delta t_{emission}$, was estimated from uncertainties in v_{wind} and d_{source}. (See the Supporting Information for further details.)

The source SO_2/CO_2 EmR corresponding with each plume encounter was estimated as the mean EmR value for the hours containing $t_{emission} \pm \delta t_{emission}$, using emissions data reported in the AMPD database (step 4, Figure 2; example data, Figure 4). Overall uncertainty in each EmR value was conservatively estimated as the sum of two values: (1) twice the EmR relative standard deviation (RSD) and (2) 14%, which was assumed to be the accuracy of the hourly EmR values, on the basis of the results of Peischl et al.[51] The observed plume SO_2/CO_2 ER was then calculated from 10 s averaged measurements by linear ODR using the script provided by Cantrell;[52] each measurement was weighted by the associated 1σ precision or by the overall uncertainty when precision was not separately provided (e.g., the weight of measured value i, W_i, was calculated as $1 - \sigma_i$, where σ_i denotes the fractional 1σ precision in i). Enhancement ratios calculated in this way are insensitive to plume dilution when the composition of the background air is approximately constant between the points of emission and sampling. Overall uncertainty in each ER value was conservatively estimated as the sum of two values: (1) the 95% CI in the ODR slope and (2) the sum in quadrature of the calibration uncertainties in the SO_2 and CO_2 measurements. A sampled plume was attributed to a particular upwind CFPP when the corresponding ER−EmR pair agreed to within

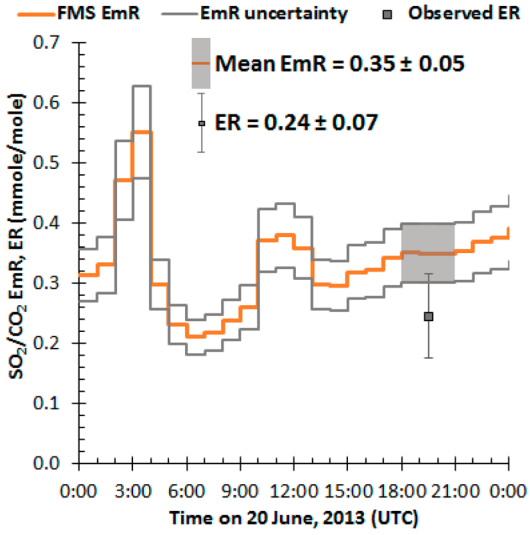

Figure 4. Hourly SO_2/CO_2 EmRs for Fort Martin Station (FMS) on June 20, 2013. For plume FMS-07-B in Table 1 (plume 2 in Figure S2), we estimate the corresponding source EmR on the basis of emissions data from the interval $t_{emission} \pm \delta t_{emission}$ (shaded area). The observed SO_2/CO_2 ER, which we consider to be directly comparable to the inventory-based EmR is plotted at the center of the estimated emission interval.

combined uncertainties. We estimate that in-plume SO_2 loss via gas-phase oxidation may have slightly reduced the plume SO_2/CO_2 ERs (by ≤14%) relative to the corresponding EmRs (Table S7). However, because adjusting the SO_2/CO_2 EmRs for estimated SO_2 oxidation would not change the conclusions from this study, no such adjustment was made. (See Supporting Information for further details.)

When the SO_2/CO_2 ER was unquantifiable (e.g., because of lack of significant CO_2 enhancement) or when this ratio (and HYSPLIT) could not discriminate between multiple CFPPs, we incorporated NO_x data into the ER−EmR pair comparisons. In

DOI: 10.1021/acs.est.5b01755
Environ. Sci. Technol. XXXX, XXX, XXX−XXX

Table 1. Comparison of Measured and Inventory-Based THg/CO_2 ratios for CFPP Plumes Sampled during NOMADSS

	Hg/CO_2 ratio (nmol/mol)				
plume ID[a]	NEI-based EmR[b]	TRI-based EmR[c]	measured ER (r^2, n)[d]	% diff. (NEI)[e,f]	% diff. (TRI)[f,g]
FMS-07-A	1.3 ± 0.2	2.5 ± 0.3	2.3 ± 1.2 (0.82, 8)*	−75	6
FMS-07-B	1.3 ± 0.2	2.5 ± 0.3	2.3 ± 1.4 (0.81, 7)*	−79	5
FMS-07-AB	1.3 ± 0.2	2.5 ± 0.3	2.3 ± 0.8 (0.81, 15)**	−77	5
HTS-07	3.4 ± 0.5	4.0 ± 0.6	2.3 ± 1.3 (0.83, 7)*	32	43
WPP-08-B	5.5 ± 0.8	4.9 ± 0.7	6.8 ± 4.4 (0.85, 6)*	−23	−39
LMS-08-A	11 ± 2	4.8 ± 0.7	15 ± 4 (0.989, 5)**	−42	**−223**
LMS-08-B	11 ± 2	4.8 ± 0.7	14 ± 4 (0.989, 5)**	−30	**−197**
LMS-08-AB	11 ± 2	4.8 ± 0.7	14 ± 3 (0.986, 7)**	−33	**−202**
		median[h]		−36	−17

[a]Plume abbreviation: III-FF-X, where III is the three-letter source identifier (Figure 1), FF is the two-digit flight number, and X denotes the plume crossing identifier (in alphabetical order) when the source was sampled twice on the same flight. For plumes labeled AB, the measured ER values were calculated from the combined data for both plume crossings. [b]Mean value calculated from Hg emissions data in the 2011 NEI and CO_2 emissions data in the AMPD database for the time period including $t_{emission} \pm \delta t_{emission}$. [c]Calculated from annual emissions of Hg (TRI) and CO_2 (AMPD) for 2013. [d]All correlations are statistically significant (f test, $p < 0.05$); *, $p < 0.01$, and **, $p < 0.001$. [e]Percent differences between the NEI-based EmRs and measured ERs; the values are calculated relative to the EmRs and are negative when EmR < ER). [f]Values in bold type are statistically significant. [g]These data are similar to those in the preceding column, but these are calculated with respect to the TRI-based EmRs. [h]Excludes data for AB plumes.

Table 2. Comparison of Measured and Inventory-Based THg/SO_2 Ratios for CFPP Plumes Sampled during NOMADSS[a]

	Hg/SO_2 ratio (μmol/mol)				
source ID[b]	NEI-based EmR[c]	TRI-based EmR[d]	measured ER (r^2, n)[e]	% diff. (NEI)[f,g]	% diff. (TRI)[g,h]
BBS-08-A	0.27 ± 0.05	2.8 ± 0.4	5.8 ± 4.8 (0.90, 5)	**−2060**	−108
BBS-08-B	0.27 ± 0.05	2.8 ± 0.4	5.2 ± 4.1 (0.86, 6)*	**−1818**	−84
DHS-13-A	3.3 ± 0.5	1.7 ± 0.2	5.4 ± 2.7 (0.92, 7)**	−62	**−218**
DHS-13-B	3.3 ± 0.5	1.7 ± 0.2	6.5 ± 2.4 (0.98, 6)**	**−97**	**−287**
DHS-13-AB	3.3 ± 0.5	1.7 ± 0.2	5.5 ± 1.9 (0.93, 13)**	−67	**−228**

[a]Emissions data for SO_2 were taken from the AMPD database. [b]Plume abbreviations: III-FF-X, where III is the three-letter source identifier (Figure 1), FF is the two-digit flight number, and X denotes the plume crossing identifier (in alphabetical order) when the source was sampled twice on the same flight. For plumes labeled AB, the measured ER values were calculated from the combined data for both plume crossings. [c]Mean value calculated from Hg emissions data in the 2011 NEI and SO_2 emissions data in the AMPD database for the time period including $t_{emission} \pm \delta t_{emission}$. [d]Calculated from annual emissions of Hg (TRI) and SO_2 (AMPD) for 2013. [e]All correlations are statistically significant (f test, $p < 0.05$); *, $p < 0.01$, and **, $p < 0.001$. [f]Percent differences between the NEI-based EmRs and measured ERs; the values are calculated relative to the EmRs and are negative when EmR < ER). [g]Values in bold type are statistically significant. [h]These data are similar to those in the preceding column, but these are calculated with respect to the TRI-based EmRs.

doing so, a process analogous to that described in the preceding paragraph was used. However, because the in-plume NO_x lifetimes were generally estimated to be comparable to Δt_{plume}, EmRs that incorporated NO_x were corrected for estimates of NO_x loss. (See Supporting Information for further details.) We did not use CO data for source identification because uncertainties in the inventoried CO emissions are larger and less well constrained than for NO_x and SO_2.[51] When the possible source was not a CFPP, it was excluded from consideration in this study.

Quantification of Hg EmRs and ERs for CFPPs. For the CFPPs we sampled, the 2011 NEI reports annual Hg emission quantities (e^{Hg}, ton/yr) derived from MATS Hg emission intensities (lb/MMBtu) and annual heat inputs (MMBtu/yr) reported in the AMPD database. Conversely, the TRI reports values of e^{Hg} (lb/yr) estimated by the emitting facilities using several methods;[48] the underlying emission intensities are not reported. We calculated NEI-based Hg/CO_2 and Hg/SO_2 EmRs as the ratios of the corresponding molar emission intensities. The CO_2 and SO_2 emission intensities were calculated for the time period including $t_{plume} \pm \delta t_{plume}$ from emissions data reported in the AMPD database, thereby incorporating real-time hourly variability in the CO_2 and SO_2 emission intensities into the calculated EmRs. We calculated TRI-based Hg/CO_2 and Hg/SO_2 EmRs as the ratios of the corresponding annual molar emission quantities, using CO_2 and SO_2 emissions data from the AMPD database. Uncertainties in the EmRs were estimated on the basis of only uncertainties in the corresponding CO_2 and SO_2 emissions data because uncertainties associated with the facility-level Hg emissions data were not characterized prior to this study.

For each CFPP plume which we identified, we calculated the associated THg/CO_2 and THg/SO_2 ERs as described above for the SO_2/CO_2 ERs, except using 2.5 min averaged measurements instead of 10 s averages. At the lower time resolution, the center of each plume was defined by 1 or 2 samples.

RESULTS AND DISCUSSION

Here, we present our source identifications for plumes we attributed to CFPPs, comparing for each plume the observed SO_2/CO_2 (or SO_2/NO_x) ER with the corresponding inventory-based EmR. We then compare the observed and inventory-based THg/CO_2 (or THg/SO_2) ratios.

Source Identifications. The CFPPs we sampled and for which we quantified the THg/CO_2 or THg/SO_2 ERs are listed in Tables 1 and 2, respectively. (See also Table S2.) These include Big Brown Station (BBS) in Texas, Dolet Hills Station (DHS) in Louisiana, Fort Martin Station (FMS) in West

DOI: 10.1021/acs.est.5b01755
Environ. Sci. Technol. XXXX, XXX, XXX−XXX

Virginia, Hatfield Station (HTS) in Pennsylvania, and Limestone Station (LMS) in Texas. (Measured SO_2/CO_2 ERs are compared in Table S3 with the corresponding source EmRs for all CFPPs in Tables 1 and 2, with the exception of Big Brown for which the SO_2/CO_2 ER was unquantifiable, as discussed below.) The Fort Martin plumes could not be assigned exclusively to Fort Martin on the basis of only the observed SO_2/CO_2 ERs. We therefore also used NO_x data to exclude a separate nearby CFPP as a source of these plumes. (See Supporting Information for further details.) For CFPPs that were sampled in duplicate (Dolet Hills, Fort Martin, and Limestone), the observed SO_2/CO_2 ERs for each plume crossing were statistically indistinguishable from one another at 95% CI; relative differences for all duplicate plume crossings were within ±9.8%, suggesting that the ERs were not greatly influenced by background variability during plume dilution.

For Big Brown Station, the SO_2/CO_2 ER could not be determined because CO_2 was not significantly enhanced in the plume, possibly because of inefficient plume penetration by the aircraft. Therefore, we carried out our source identification using the SO_2/NO_x ratio, after correcting the corresponding SO_2/NO_x EmR values for estimated NO_x loss. (See Supporting Information for further details.) The measured and corrected inventory-based SO_2/NO_x ratios are compared in Table S4. The measured SO_2/NO_x ratios are consistent with the inventory values, with or without correction for NO_x loss, and are statistically indistinguishable from one another at 95% CI (relative difference = ±56%, possibly reflecting unaccounted for variability in either the NO_x background or plume chemistry).

Hg EmRs and ERs. For each CFPP plume, the observed THg/CO_2 ER is compared with the associated inventory-based EmR in Table 1. The Dolet Hills Station plumes are excluded from Table 1 because the observed THg/CO_2 correlations were not statistically significant at 95% CI (p = 0.090 and 0.68 for the A and B plumes, respectively). For CFPPs that were sampled in duplicate (Fort Martin Station and Limestone Station), the observed ERs for each plume crossing were statistically indistinguishable from one another at the 95% CI (relative differences were within ±8.6%). For these CFPPs, we determined the THg/CO_2 ERs with smaller relative uncertainty by performing regression analysis on the combined data for both plume crossings (plumes labeled AB in Table 1).

For the plumes attributed to Dolet Hills Station and Big Brown Station, the THg/SO_2 ERs are compared to the corresponding inventory-based values in Table 2. (Similar data for the plumes in Table 1 are given in Table S8.) The THg/SO_2 ERs measured for duplicate plume crossings were statistically indistinguishable at 95% CI (relative differences were within ±19%). For Dolet Hills, we determined the THg/SO_2 ER with smaller relative uncertainty by performing regression analysis on the combined data for both plume crossings (plume labeled AB in Table 2).

Comparisons between Observed Hg ERs and Inventory-Based Hg EmRs. Percent differences between each observed THg/CO_2 ER and the corresponding NEI- and TRI-based EmRs, relative to the inventory-based values (i.e., percent difference =100 × (EmR − ER) ÷ EmR), are given in the last two columns of Table 1. Analogous results for the THg/SO_2 ER−EmR pairs are given in Table 2. Negative percent differences correspond with ER > EmR, and values in bold type are larger than the combined uncertainties for the ER−EmR pair. (The analysis does not account for uncertainties in the associated Hg emissions data nor does it account for short-term variability in the Hg emission intensities, discussed further in Supporting Information.)

Composite Comparisons. Linear regression of the measured versus NEI-based THg/CO_2 ratios (Figure 5),

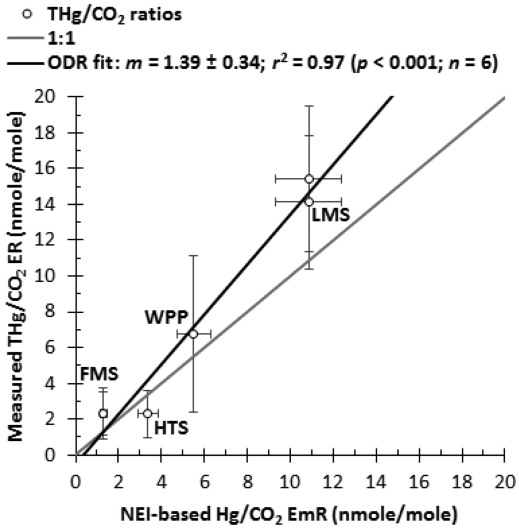

Figure 5. Linear regression of measured THg/CO_2 ERs against 2011 NEI-based EmRs for CFPP plumes sampled during NOMADSS (plumes listed in Table 1; excluding AB plumes). Uncertainty in the slope is 95% CI. Error bars represent uncertainties in Table 1.

including the data in Table 1 (excluding the AB plumes), yields a strong correlation (r^2 = 0.97, p < 0.001, n = 6), with a slope of 1.39 ± 0.34 nmol/mol (95% CI) and a nonsignificant intercept at the 95% CI (−0.5 ± 2.5). These results suggest that the 2011 NEI data tended to underestimate Hg emissions from the CFPPs we sampled, with an overall bias of −39%. Similarly, the median percent difference between measured and NEI-based THg/CO_2 ratios (Table 1, excluding the AB plumes) is −36%, although none of the individual differences between measured and NEI-based THg/CO_2 ratios were statistically significant. The NEI-based THg/SO_2 ratios in Table 2 also tend to be biased low compared with the measured values, especially for Big Brown Station (percent difference of approximately −2000%; discussed below).

The measured THg/CO_2 ratios were not correlated with the 2013 TRI-based values at 95% CI (p = 0.09). This result appears to be largely driven by the Limestone ER−EmR pair, in which the TRI-based value is significantly lower than the ERs we measured (Table 1). Although exclusion of Limestone Station did not yield a significant linear correlation at 95% CI (p = 0.2, n = 4), substitution of the 2011 TRI data yielded a slope of 2.1 ± 0.6 and an intercept of −3.7 ± 3.5 nmol/mol (r^2 = 0.96, p < 0.001). The median percent difference between measured and TRI-based THg/CO_2 ratios (excluding AB plumes) is −17%. The TRI-based THg/SO_2 ratios in Table 2 also tend to be biased low compared with the measured values. The TRI therefore appears to be of limited value as a quantitative tool for the prediction of real-time Hg emissions at individual CFPPs, at least for the facilities considered here.

Facility-Level Comparisons. For Limestone Station, our measurements (and the NEI-based EmR) are more consistent with the 2011 TRI-based EmR (8.9 ± 1.2 nmol/mol), which is much larger than the 2013 TRI value (Table 1). The TRI

DOI: 10.1021/acs.est.5b01755
Environ. Sci. Technol. XXXX, XXX, XXX−XXX

indicates that total environmental Hg releases (atmospheric emissions + on-site land disposal) at Limestone were 0.82 tons/yr in 2011 and only slightly lower (by <10%) in 2013. However, the quantity of atmospheric emissions in the TRI decreased significantly from 73% of the total in 2011 to 40% in 2013, implying a concomitant improvement in Hg removal efficiency for the emissions controls employed. (Neither the TRI nor the AMPD database indicate a change in emissions controls at Limestone between 2011 and 2013.) The TRI further indicates that published EmRs were used to estimate atmospheric Hg emissions at Limestone in both 2011 and 2013. Although the EmR values are not explicitly stated, it appears that a lower EmR was used to calculate the 2013 TRI emissions, and this value is biased low with respect to our measurements during NOMADSS.

Hatfield Station and Welsh Power Plant are the only CFPPs we sampled for which the MATS Hg emission intensities were derived from on-site emissions measurements. The THg/CO_2 ratios we measured for these facilities exhibited some of the lowest percent differences with respect to the corresponding NEI-based EmRs (Table 1). This indicates that Hg emissions data are more reliable when they are traceable to on-site emissions measurements.

Considering the THg/SO_2 ER–EmR pairs in Table 2, the measured ERs significantly disagree with one of the inventory-based EmRs for both Big Brown Station and Dolet Hills Station. For Dolet Hills, the measured ratio is marginally consistent with the NEI-based value but is significantly larger than the TRI-based value. The TRI indicates that site-specific EmRs were used to estimate atmospheric Hg emissions at Dolet Hills in both 2011 and 2013. The 2011 and 2013 TRI-based THg/CO_2 EmRs agree to within ±1%, indicating that the same EmR was likely used in both years. It appears that the EmR was not derived from on-site emissions measurements. The MATS Hg emission intensity for Dolet Hills, which is used in the NEI, also was not derived from on-site emissions measurements but appears to be reasonably accurate in this case.

For Big Brown Station, the measured THg/SO_2 ratio is consistent with the TRI-based value, but is significantly larger than the NEI-based value. The apparent low bias in the NEI-based EmR implies an underestimation of the corresponding emission intensity. The MATS Hg emission intensity for Big Brown represents the mean value derived from emissions measurements carried out at 17 separate CFPPs having similar characteristics in terms of fuel type, boiler type, and emissions controls. For these 17 CFPPs, the MATS emission intensities vary widely, spanning more than 2 orders of magnitude (3.43×10^{-8}–6.41×10^{-6} lb/MMBtu, RSD = 130%), and the mean value is highly uncertain when applied to individual CFPPs. The THg/SO_2 ERs we measured for Big Brown are consistent (to within measurement uncertainties) with Hg emission intensities $\geq 4.8 \times 10^{-6}$ lb/MMBtu, which is near the high end of the range of values underlying the NEI-based EmR. (By comparison, the TRI-based THg/SO_2 EmR corresponds with an even larger Hg emission intensity of 1.3×10^{-5} lb/MMBtu.) It is therefore likely that the emission intensity applied to Big Brown in the NEI is much lower than the true value. Our results indicate that the prescription of Hg emission intensities to untested CFPPs can in some cases lead to very large errors in the corresponding emissions estimates.

Our results further suggest that efforts to improve the Hg emissions inventories should pay special attention to CFPPs for which the NEI and TRI are in large disagreement. For such cases, we show that plume measurements from an aircraft platform can identify outlying emissions estimates. We recommend that future Hg emission inventories provide greater traceability as to how emissions are calculated for each facility and provide an estimate of uncertainty.

■ ASSOCIATED CONTENT

Supporting Information

Details on Hg emissions estimates, the DOHGS instrument, emissions inventories, analysis methods, plume attribution results, estimation of short-term variability in Hg emission intensities, THg/SO_2 ER–EmR comparisons. The Supporting Information is available free of charge on the ACS Publications website at DOI: 10.1021/acs.est.5b01755.

■ AUTHOR INFORMATION

Corresponding Author

*Phone: (603) 988-2473. E-mail: jambrose@alumni.unh.edu.

Present Addresses

J.L.A.: P.O. Box 95, New Castle, NH 03854, United States.
D.M.S.: Department of Atmospheric Sciences, University of Illinois, Urbana, IL, 61801, United States.
M.S.: Department of Earth and Atmospheric Sciences, Metropolitan State University of Denver, Denver, CO, 80217, United States

Funding

This work was funded by the U.S. National Science Foundation.

Notes

The authors declare no competing financial interest.

■ ACKNOWLEDGMENTS

Our participation in the NOMADSS experiment was sponsored by the NSF (award nos.: 1216743 and 1217010) and conducted as part of the Southeast Atmosphere Study, which was also primarily sponsored by the NSF. The involvement of the NSF-sponsored Lower Atmospheric Observing Facilities, managed and operated by the National Center for Atmospheric Research's Earth Observing Laboratory, is acknowledged. We thank Allen Hart (University of Washington, Seattle) and Jonathan Hee (UW, Bothell) for their assistance. We also thank four anonymous reviewers for helpful critiques of the original manuscript.

■ ABBREVIATIONS

AMPD	Air Markets Program Data
AMSL	above mean sea level
CAP	criteria air pollutant
CEM	cation exchange membrane
CFPP	coal-fired power plant
CI	confidence interval
CIMS	chemical ionization mass spectrometry
DOHGS	detector for oxidized Hg species
EPA	Environmental Protection Agency
EmR	emission ratio
ER	enhancement ratio
GEM	gaseous elemental mercury
GHGRP	Greenhouse Gas Reporting Program
HAP	hazardous air pollutant
HYSPLIT	HYbrid Single-Particle Lagrangian Integrated Trajectory

DOI: 10.1021/acs.est.5b01755
Environ. Sci. Technol. XXXX, XXX, XXX–XXX

MATS	Mercury and Air Toxics Standards
NCAR	National Center for Atmospheric Research
NEI	National Emissions Inventory
NOAA	National Oceanic and Atmospheric Administration
NOMADSS	Nitrogen, Oxidants, Mercury, and Aerosol Distributions, Sources, and Sinks
NSF	National Science Foundation
ODR	orthogonal distance regression
RF	research flight
RSD	relative standard deviation
SAS	Southeast Atmosphere Study
THg	total mercury
TRI	Toxics Release Inventory

REFERENCES

(1) Pacyna, E. G.; Pacyna, J. M. Global emission of mercury from anthropogenic sources in 1995. *Water, Air, Soil Pollut.* **2002**, *137*, 149−165.

(2) Pacyna, E. G.; Pacyna, J. M.; Steenhuisen, F.; Wilson, S. Global anthropogenic mercury emission inventory for 2000. *Atmos. Environ.* **2006**, *40*, 4048−4063.

(3) Pacyna, E. G.; Pacyna, J. M.; Sundseth, K.; Munthe, J.; Kindbom, K.; Wilson, S.; Steenhuisen, F.; Maxson, P. Global emission of mercury to the atmosphere from anthropogenic sources in 2005 and projections to 2020. *Atmos. Environ.* **2010**, *44*, 2487−2499.

(4) Streets, D. G.; Zhang, Q.; Wu, Y. Projections of global mercury emissions in 2015. *Environ. Sci. Technol.* **2009**, *43*, 2983−2988.

(5) Pirrone, N.; Cinnirella, S.; Feng, X.; Finkelman, R. B.; Friedli, H. R.; Leaner, J.; Mason, R.; Mukherjee, A. B.; Stracher, G. B.; Streets, D. G.; Telmer, K. Global mercury emissions to the atmosphere from anthropogenic and natural sources. *Atmos. Chem. Phys.* **2010**, *10*, 5951−5964.

(6) Chen, Y.; Wang, R.; Shen, H.; Li, W.; Chen, H.; Huang, Y.; Zhang, Y.; Chen, Y.; Su, S.; Lin, N.; Liu, J.; Li, B.; Wang, X.; Liu, W.; Coveney, R. M., Jr.; Tao, S. Global mercury emissions from combustion in light of international fuel trading. *Environ. Sci. Technol.* **2014**, *48*, 1727−1735.

(7) U.S. Environmental Protection Agency *2011 National Emissions Inventory, Version 1 Technical Support Document − Draft*; Technical report prepared for the U.S. Environmental Protection Agency, Office of Air Quality Planning and Standards, Air Quality Assessment Division, Emissions Inventory and Analysis Group: Research Triangle Park, NC, 2014. http://www.epa.gov/ttn/chief/net/2011nei/2011_nei_tsdv1_draft2_june2014.pdf (accessed December 22, 2014).

(8) Pacyna, J. M.; Pacyna, E. G.; Steenhuisen, F.; Wilson, S. Mapping 1995 global anthropogenic emissions of mercury. *Atmos. Environ.* **2003**, *37* (S1), 109−117.

(9) Wilson, S. J.; Steenhuisen, F.; Pacyna, J. M.; Pacyna, E. G. Mapping the spatial distribution of global anthropogenic mercury atmospheric emission inventories. *Atmos. Environ.* **2006**, *40*, 4621−4632.

(10) Lindberg, S. E.; Bullock, R.; Ebinghaus, R.; Engstrom, D.; Feng, X.; Fitzgerald, W.; Pirrone, N.; Prestbo, E.; Seigneur, C. A synthesis of progress and uncertainties in attributing the sources of mercury in deposition. *Ambio* **2007**, *36*, 19−32.

(11) Swain, E. B.; Jakus, P. M.; Rice, G.; Lupi, F.; Maxson, P. A.; Pacyna, J. M.; Penn, A.; Spiegel, S. J.; Veiga, M. M. Socioeconomic consequences of mercury use and pollution. *Ambio* **2007**, *36*, 45−61.

(12) Selin, N. E. Global biogeochemical cycling of mercury: A review. *Annu. Rev. Env. Resour* **2009**, *34*, 43−63.

(13) Edgerton, E. S.; Hartsell, B. E.; Jansen, J. J. Mercury speciation in coal-fired power plant plumes observed at three surface sites in the southeastern U.S. *Environ. Sci. Technol.* **2006**, *40*, 4563−4570.

(14) Lohman, K.; Seigneur, C.; Edgerton, E.; Jansen, J. Modeling mercury in power plant plumes. *Environ. Sci. Technol.* **2006**, *40*, 3848−3854.

(15) Amos, H. M.; Jacob, D. J.; Holmes, C. D.; Fisher, J. A.; Wang, Q.; Yantosca, R. M.; Corbitt, E. S.; Galarneau, E.; Rutter, A. P.; Gustin, M. S.; Steffen, A.; Schauer, J. J.; Graydon, J. A.; St. Louis, V. L.; Talbot, R. W.; Edgerton, E. S.; Zhang, Y.; Sunderland, E. M. Gas-particle partitioning of atmospheric Hg(II) and its effects on global mercury deposition. *Atmos. Chem. Phys.* **2012**, *12*, 591−603.

(16) Timonen, H.; Ambrose, J. L.; Jaffe, D. A. Oxidation of elemental Hg in anthropogenic and marine airmasses. *Atmos. Chem. Phys.* **2013**, *13*, 2827−2836.

(17) Zhang, Y.; Jaeglé, L.; van Donkelaar, A.; Martin, R. V.; Holmes, C. D.; Amos, H. M.; Wang, Q.; Talbot, R.; Artz, R.; Brooks, S.; Luke, W.; Holsen, T. M.; Felton, D.; Miller, E. K.; Perry, K. D.; Schmeltz, D.; Steffen, A.; Tordon, R.; Weiss-Penzias, P.; Zsolway, R. Nested-grid simulation of mercury over North America. *Atmos. Chem. Phys.* **2012**, *12*, 6095−6111.

(18) Kos, G.; Ryzhkov, A.; Dastoor, A.; Narayan, J.; Steffen, A.; Ariya, P. A.; Zhang, L. Evaluation of discrepancy between measured and modelled oxidized mercury species. *Atmos. Chem. Phys.* **2013**, *13*, 4839−4863.

(19) Deeds, D. A.; Banic, C. M.; Lu, J.; Daggupaty, S. Mercury speciation in a coal-fired power plant plume: An aircraft-based study of emissions from the 3640MW Nanticoke Generating Station, Ontario, Canada. *J. Geophys. Res. Atmos.* **2013**, *118*, 4919−4935.

(20) Landis, M. S.; Ryan, J. V.; ter Schure, A. F. H.; Laudal, D. Behavior of Mercury Emissions from a Commercial Coal-Fired Power Plant: The Relationship between stack speciation and near-field plume measurements. *Environ. Sci. Technol.* **2014**, *48*, 13540−13548.

(21) Pacyna, J. M.; Pacyna, E. G.; Aas, W. Changes of emissions and atmospheric deposition of mercury, lead, and cadmium. *Atmos. Environ.* **2009**, *43*, 117−127.

(22) French, C. L.; Maxwell, W. H.; Peters, W. D.; Rice, G. E.; Bullock, O. R.; Vasu, A. B.; Hetes, R.; Colli, A.; Nelson, C.; Lyons, B. F.; French, C. L.; et al. *Study of Hazardous Air Pollutant Emissions from Electric Utility Steam Generating Units − Final Report to Congress, Volume 1*; Technical Report no. EPA-453/R-98-004a prepared for the U.S. Office of Air Quality, Environmental Protection Planning and Standards Agency: Research Triangle Park, NC, 1998. http://www.epa.gov/ttn/atw/combust/utiltox/eurtc1.pdf (accessed April 3, 2015).

(23) U.S. Environmental Protection Agency *Technology Transfer Network Clearinghouse for Inventories & Emissions Factors Home Page.* http://www.epa.gov/ttn/chief/eiinformation.html (accessed February 3, 2015).

(24) U.S. Environmental Protection Agency *Toxics Release Inventory (TRI) Program Home Page*. http://www2.epa.gov/toxics-release-inventory-tri-program (accessed February 21, 2015).

(25) U.S. Environmental Protection Agency *Documentation for the Final 2002 Point Source National Emissions Inventory*; U.S. Environmental Protection Agency, Air Quality and Analysis Division, Emission Inventory and Analysis Group: Research Triangle Park, NC, 2006. ftp://ftp.epa.gov/EmisInventory/2002finalnei/documentation/point/2002nei_final_point_source_documentation0206.pdf (accessed December 13, 2014).

(26) Seigneur, C.; Vijayaraghavan, K.; Lohman, K. Atmospheric mercury chemistry: Sensitivity of global model simulations to chemical reactions. *J. Geophys. Res.* **2006**, *111*, D22305 DOI: 10.1029/2005JD006780.

(27) Sillman, S.; Marsik, F. J.; Al-Wali, K. I.; Keeler, G. J.; Landis, M. S. Reactive mercury in the troposphere: Model formation and results for Florida, the northeastern United States, and the Atlantic Ocean. *J. Geophys. Res.* **2007**, *112*, D23305 DOI: 10.1029/2006JD008227.

(28) Pongprueksa, P.; Lin, C. J.; Lindberg, S. E.; Jang, C.; Braverman, T.; Bullock, O. R.; Ho, T. C.; Chu, H. W. Scientific uncertainties in atmospheric mercury models III: Boundary and initial conditions, model grid resolution, and Hg(II) reduction mechanism. *Atmos. Environ.* **2008**, *42*, 1828−1845.

(29) Vijayaraghavan, K.; Karamchandani, P.; Seigneur, C.; Balmori, R.; Chen, S.-Y. Plume-in-grid modeling of atmospheric mercury. *J. Geophys. Res.* **2008**, *113*, D24305 DOI: 10.1029/2008JD010580.

DOI: 10.1021/acs.est.5b01755
Environ. Sci. Technol. XXXX, XXX, XXX−XXX

(30) Weiss-Penzias, P.; Amos, H. M.; Selin, N. E.; Gustin, M. S.; Jaffe, D. A.; Obrist, D.; Sheu, G.-R.; Giang, A. Use of a global model to understand speciated atmospheric mercury observations at five high-elevation sites. *Atmos. Chem. Phys.* **2015**, *15*, 1161−1173.
(31) Holmes, C. D.; Jacob, D. J.; Corbitt, E. S.; Mao, J.; Yang, X.; Talbot, R.; Slemr, F. Global atmospheric model for mercury including oxidation by bromine atoms. *Atmos. Chem. Phys.* **2010**, *10*, 12037−12057.
(32) *Southeast Atmosphere Study Home Page*. http://www.eol.ucar.edu/field_projects/sas (accessed February 21, 2015).
(33) Gratz, L. E.; Shah, V.; Ambrose, J. L.; Jaffe, D. A.; Jaeglé, L.; Stutz, J.; Festa, J.; Spolaor, M.; Tsai, C.; Selin, N. E.; Song, S.; Zhou, X.; Weinheimer, A.; Knapp, D. J.; Montzka, D. D.; Flocke, F. M.; Campos, T. L.; Apel, E.; Hornbrook, R.; Blake, N. J.; Hall, S.; Tyndall, G. S.; Reeves, M.; Stechman, D.; Stell, M. Oxidation of mercury by bromine in the subtropical Pacific free troposphere, *Nature Geosci.*, submitted for publication, **2015**.
(34) Shah, V.; Jaeglé, L.; Gratz, L.; Ambrose, J. L. II; Jaffe, D. A. NOMADSS Aircraft Observations Suggest Rapid Oxidation of Elemental Mercury in the Subtropical Free Troposphere; presented at 2014 AGU Fall Meeting, San Francisco, CA, December 15−19, 2014; American Geophysical Union: Washington, D.C., 2014; Abstract B43F-0298.
(35) Song, S.; Selin, N. E.; Jaffe, D. A.; Jaeglé, L.; Gratz, L.; Ambrose, J. L. II; Shah, V.; Giang, A. Use of NOMADSS Observations to Improve Our Understanding of the Land and Ocean Fluxes of Mercury. Presented at 2014 AGU Fall Meeting, San Francisco, CA, December 15−19, 2014; American Geophysical Union: Washington, D.C., 2014; Abstract A32A-07.
(36) Ambrose, J. L.; Lyman, S. N.; Huang, J.; Gustin, M. S.; Jaffe, D. A. Fast time resolution oxidized mercury measurements during the Reno Atmospheric Mercury Intercomparison Experiment (RAMIX). *Environ. Sci. Technol.* **2013**, *47*, 7285−7294.
(37) Lyman, S. N.; Jaffe, D. A. Formation and fate of oxidized mercury in the upper troposphere and lower stratosphere. *Nat. Geosci.* **2011**, *5*, 114−117.
(38) Landis, M. S.; Stevens, R. K.; Schaedlich, F.; Prestbo, E. M. Development and characterization of an annular denuder methodology for the measurement of divalent inorganic reactive gaseous mercury in ambient air. *Environ. Sci. Technol.* **2002**, *36*, 3000−3009.
(39) Ridley, B. A.; Grahek, F. E. A small, low flow, high sensitivity reaction vessel for NO chemiluminescence detectors. *J. Atmos. Oceanic Technol.* **1990**, *7*, 307−311.
(40) Pollack, I. B.; Ryerson, T. B.; Trainer, M.; Parrish, D. D.; Andrews, A. E.; Atlas, E. L.; Blake, D. R.; Brown, S. S.; Commane, R.; Daube, B. C.; de Gouw, J. A.; Dubé, W. P.; Flynn, J.; Frost, G. J.; Gilman, J. B.; Grossberg, N.; Holloway, J. S.; Kofler, J.; Kort, E. A.; Kuster, W. C.; Lang, P. M.; Lefer, B.; Lueb, R. A.; Neuman, J. A.; Nowak, J. B.; Novelli, P. C.; Peischl, J.; Perring, A. E.; Roberts, J. M.; Santoni, G.; Schwarz, J. P.; Spackman, J. R.; Wagner, N. L.; Warneke, C.; Washenfelder, R. A.; Wofsy, S. C.; Xiang, B. Airborne and ground-based observations of a weekend effect in ozone, precursors, and oxidation products in the California South Coast Air Basin. *J. Geophys. Res.* **2012**, *117*, D00V05.
(41) Mauldin, R. L., III; Frost, G. J.; Chen, G.; Tanner, D. J.; Prevot, A. S. H.; Davis, D. D.; Eisele, F. L. OH measurements during the First Aerosol Characterization Experiment (ACE 1): Observations and model comparisons. *J. Geophys. Res.* **1998**, *103* (D13), 16713−16729.
(42) *C-130 Investigator Handbook*; Technical Report for the National Center for Atmospheric Research/University Corporation for Atmospheric Research, Earth Observing Laboratory: Boulder, CO; Table 6.1. https://www.eol.ucar.edu/system/files/c130handbook.chapter6_tables.1.pdf (accessed November 24, 2014).
(43) Schanot, A. National Center for Atmospheric Research, Boulder, CO. Personal communication, 2015.
(44) U.S. Environmental Protection Agency *Air Markets Program Data Home Page*. http://ampd.epa.gov/ampd/ (accessed February 13, 2015).
(45) U.S. Environmental Protection Agency *Greenhouse Gas Reporting Program Home Page*. http://www.epa.gov/ghgreporting/ (accessed February 21, 2015).
(46) U.S. Environmental Protection Agency *Factors to Consider when Using Toxics Release Inventory Data*; U.S. Environmental Protection Agency: Washington, D.C., 2013. http://www2.epa.gov/sites/production/files/2015-06/documents/factors_to_consider_6.15.15_final.pdf (accessed July 20, 2015).
(47) U.S. Environmental Protection Agency *Technology Transfer Network − Air Toxics Website Home Page*. http://www.epa.gov/ttn/atw/utility/utilitypg.html (accessed November 24, 2014).
(48) U.S. Environmental Protection Agency *Toxic Chemical Release Inventory Reporting Forms and Instructions (Revised 2013 Version)* [Online]; Technical Report no. EPA 260-R-14-001; U.S. Environmental Protection Agency: Washington, D.C., 2014.http://www2.epa.gov/sites/production/files/2014-02/documents/rfi_ry2013_120413.pdf (accessed December 10, 2014).
(49) U.S. Environmental Protection Agency *Documentation for the Final 2002 Point Source National Emissions Inventory*; U.S. Environmental Protection Agency, Emission Inventory and Analysis Group, Air Quality and Analysis Division: Research Triangle Park, NC, 2006.
(50) Draxler, R. R.; Rolph, G. D. *HYSPLIT (HYbrid Single-Particle Lagrangian Integrated Trajectory) Model*; NOAA Air Resources Laboratory: Silver Spring, MD. http://www.arl.noaa.gov/HYSPLIT.php (accessed via NOAA ARL READY Web Page February 13, 2015).
(51) Peischl, J.; Ryerson, T. B.; Holloway, J. S.; Parrish, D. D.; Trainer, M.; Frost, G. J.; Aikin, K. C.; Brown, S. S.; Dubé, W. P.; Stark, H.; Fehsenfeld, F. C. A top-down analysis of emissions from selected Texas power plants during TexAQS 2000 and 2006. *J. Geophys. Res.* **2010**, *115*, D16303 DOI: 10.1029/2009JD013527.
(52) Cantrell, C. A. Technical Note: Review of methods for linear least-squares fitting of data and application to atmospheric chemistry problems. *Atmos. Chem. Phys.* **2008**, *8*, 5477−5487.

DOI: 10.1021/acs.est.5b01755
Environ. Sci. Technol. XXXX, XXX, XXX−XXX